ACS APPLIED MATERIALS & INTERFACES

Research Article

www.acsami.org

Adhesion of Adipose-Derived Mesenchymal Stem Cells to Glycosaminoglycan Surfaces with Different Protein Patterns

Diana Soares da Costa,*[,†,‡] Maria del Carmen Márquez-Posadas,[§,∥] Ana R. Araujo,[†,‡] Yuan Yang,[⊥] Santos Merino,[§,∥] Thomas Groth,[⊥] Rui L. Reis,[†,‡] and Iva Pashkuleva*[,†,‡]

[†]3B's Research Group, University of Minho, Headquarters of the European Institute of Excellence on Tissue Engineering and Regenerative Medicine, AvePark, 4806-909 Taipas, Guimarães, Portugal

[‡]ICVS/3B's − PT Government Associate Laboratory, Braga, Guimarães, Portugal

[§]IK4-Tekniker, Micro and Nano Manufacture Unit, Polo Tecnológico De Eibar, C/Iñaki Goenaga 5, 20600 Eibar, Gipuzkoa Spain

[∥]CIC microGUNE, Polo de Innovación Garaia, Goiru kalea 9, 20500 Arrasate-Mondragón, Gipuzkoa Spain

[⊥]Biomedical Materials Group, Martin Luther University, Heinrich-Damerow-Strasse 4, 06120 Halle (Saale), Saxony-Anhalt, Germany

Supporting Information

ABSTRACT: Proteins and glycosaminoglycans (GAGs) are the main constituents of the extracellular matrix (ECM). They act in synergism and are equally critical for the development, growth, function, or survival of an organism. In this work, we developed surfaces that display these two classes of biomacromolecules, namely, GAGs and proteins, in a spatially controlled fashion. The generated surfaces can be used as a minimalistic but straightforward model aiding the elucidation of cell−ECM interactions. GAGs (hyaluronic acid and heparin) were covalently bound to amino functionalized surfaces, and albumin or fibronectin was patterned by microcontact printing on top of them. We demonstrate that adipose-derived stem cells (ASCs) can adhere either on the protein or on the GAG pattern as a function of the patterned molecules. ASCs found on the GAG pattern had different morphology and expressed different surface markers than the cells adhered on the protein pattern. ASCs morphology and spreading were also dependent on the size of the pattern. These results show that the developed supports can also be used for ASCs differentiation into different lineages.

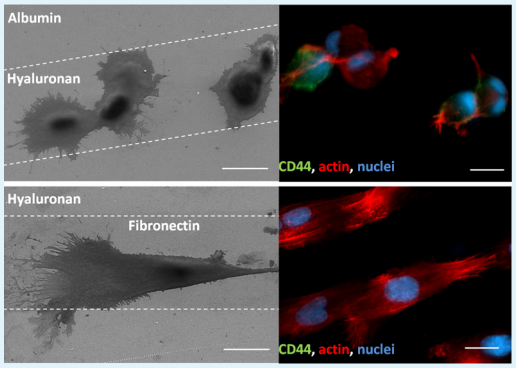

KEYWORDS: *glycosaminoglycans, adipose-derived stem cells, micropatterning, CD44*

1. INTRODUCTION

The human body contains a variety of adult stem cells capable of both repeated self-renewal and production of specialized, differentiated progeny. Discovered first in the bone marrow, mesenchymal stem cells (MSCs) demonstrated their potential for the regenerative medicine back in the 60s, when a formation of bone tissue from these cells was observed by Friedenstein and co-workers.[1] The ability of MSCs to generate tissue *de novo* following disease or injury has motivated an intensive investigation focusing on primary bone marrow stem cells (BMSC) and making them a standard for applications as tissue engineering and regenerative medicine.[2,3] Besides the identification of the characteristic stemness markers and optimization of the conditions for culturing of BMSCs, this investigation has also resulted in the identification of new sources of MSCs. Among different possibilities, adipose tissue emerged as an attractive stem cell source as the adipose-derived stem cells (ASCs) have several advantages such as multipotential differentiation similar to BMSCs, simpler isolation, and much easier access to subcutaneous adipose tissue when compared to bone marrow.[4,5] ASCs share many of the characteristics of their counterparts in bone marrow including extensive proliferative potential and the ability to undergo multilineage differentiation.[5−7] The cell surface phenotype of human ASCs is also similar to BMSCs. Both MSCs populations consistently express markers commonly associated with multilineage differentiation potential (CD105, STRO-1, and CD166) as well as several other molecules such as CD44 (hyaluronic acid receptor, crucial in the development of neoextracellular matrix) and CD49e (alpha-5 integrin, important for cell adhesion to fibronectin) and lack the expression of known hematopoietic and endothelial markers.[5,7−10]

In the last years, efforts have been mainly focused on the identification of factors that regulate MSCs differentiation, growth, and phenotypic expression. Typically, the stem cell fate is controlled by addition of soluble genetic and molecular mediators (e.g., growth factors, transcription factors) either *in vivo* or *in vitro*. However, increasing evidence shows that a

Received: March 20, 2015
Accepted: April 22, 2015
Published: April 22, 2015

DOI: 10.1021/acsami.5b02479
ACS Appl. Mater. Interfaces 2015, 7, 10034−10043

multifarious array of supplementary environmental factors contributes to the overall control of stem cell activity. Among those, the cell "'solid-state"' environment, i.e., their extracellular matrix (ECM), has a significant impact on stem cell fate. The ECM, initially considered only as a structural scaffold, is able to modulate cell behavior through mechanical signals caused by differences in ECM elasticity and morphology at the micro- and nanoscale and via specific interactions of ECM ligands with cell surface receptors[11,12]

ECM is a complex assembly that undergoes constant remodeling. It provides a wealth of bioinformation coded by glycosaminoglycans (GAGs), proteoglycans, and other soluble molecules, such as trapped and sequestered growth factors and cytokines. GAGs and proteins also play a key role in signal transduction processes at the cell surface. Therefore, cell behavior is directly or indirectly influenced by the positioning, activities, and interplay between these two classes of biomacromolecules.[13]

Herein, we describe a simple and straightforward method for the generation of micropatterned surfaces comprised by proteins and GAGs. While patterned surfaces with each of these classes of biomolecules are widely reported and used to elucidate different biointeractions,[14−16] their simultaneous surface presentation has not been previously reported. Among the proteins, we have selected the abundant, relatively small and globular albumin that is often used as a model for nonadhesive protein and fibronectin, which is well-known for its cell adhesive properties.[17] The GAG heparin (HEP) was chosen because (i) it has binding domains for fibronectin and (ii) it is the biomacromolecule with the highest negative charge due to the high degree of sulfation. On the other hand, hyaluronan (HA) was also studied because it is the only nonsulfated GAG that is secreted by the cells alone without protein conjugation. We expected therefore that these two GAGs will interact differently with the patterned protein (different stability of the pattern) and cells.

2. MATERIALS AND METHODS

Unless otherwise stated, chemicals were bought from Sigma-Aldrich and used without further purification.

2.1. Glycosaminoglycans (GAGs): Modification and Characterization. Hyaluronic acid (HA, M_w = 1.3 MDa, Kraeber & Co. GmbH, Germany) and heparin (HEP, M_w = 15 kDa, Serva) were used in this study. Functionalization with aldehyde groups was performed by oxidation of the C2 and C3 hydroxyl groups of the hexoses (either a uronic acid or glycosamine) using sodium periodate (Figure 1A) adapting a previously reported method.[18]

Briefly, GAG (0.5 g) was dissolved in 80 mL of H_2O and a different amount of sodium periodate ($NaIO_4$) was added to the solutions (Table S1, Supporting Information). The reaction was carried out at dark under stirring for 6 h. The products (ox-GAGs) were dialyzed (Spectra/Por membrane with cutoff 3500, Carl Roth, Germany) against distilled water for 3 days, freeze-dried, and characterized (Figure S1, Supporting Information) or kept at 4 °C until used. The amount of aldehydes (degree of oxidation, Do) on the ox-GAG backbone was determined by UV−vis spectroscopy (λ = 550 nm within 40 min) using Schiff's reagent. The calibration curve was established with glutaraldehyde as a standard. Schiff's reagent (2.5 mL) was added to each sample of ox-GAG (0.5 mL), and the absorbance was measured at 550 nm within 40 min. The molecular weight and polydispersity of the oxidized products (ox-GAGs) were measured by asymmetrical flow field-flow fractionation (FFFF) equipped with a Dawn EOS detector (Wyatt Technology Corp.) and a RI-Detector (Shodex, RI-101). All samples were dissolved in 50 mM NaCl containing 0.02% NaN_3 (w/v) to prevent bacteria growth. Molecular weights were calculated using Astra software (Wyatt Technology Corp.).

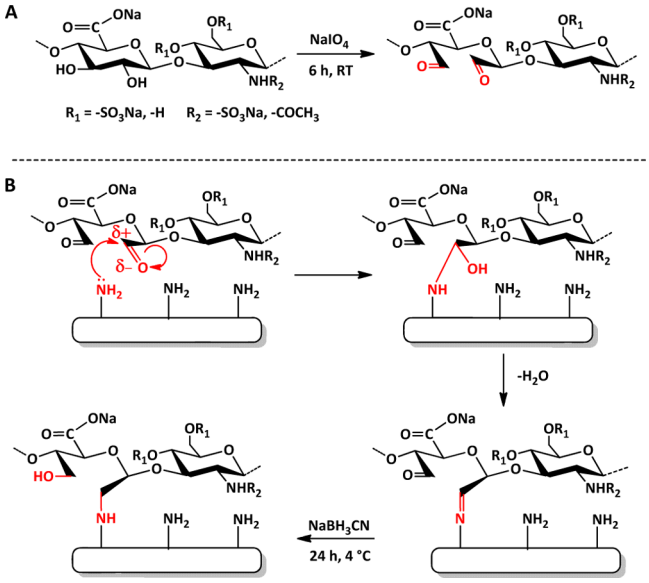

Figure 1. Schematic presentation of the glycosaminoglycan oxidation (A) and the following immobilization of the obtained aldehydes (ox-GAGs) on the amino-functionalized surfaces via Schiff base reaction (B).

2.2. Surfaces Functionalized with Glycosaminoglycans. The substrates used in this study were glass slides uniformly coated with a thick gold layer (~40 nm) by the electron beam physical vapor deposition (ATC Orion series UHV Evaporation system, AJA International Inc.). A titanium film (3 nm thick) was used as a primer improving the adhesion between the gold and the glass. Self-assembling monolayers (SAMs) were formed by immersion of cleaned substrates (piranha solution, 30 min) into 20 μM ethanol solution of $HS(CH_2)_{11}NH_2$ for at least 48 h to ensure well-organized monolayers. (CAUTION: "Piranha" solution reacts violently with organic materials; it must be handled with extreme care.) The obtained amino SAMs reacted with the generated aldehyde groups that are randomly distributed along the GAG chains via a Schiff base reaction (Figure 1B). The substrates with SAMs were immersed in a solution of ox-GAGs (4.0 mg/mL in phosphate buffer saline, PBS) for 24 h at RT followed by a reduction of the formed Schiff's base with $NaBH_3CN$ (3.0 mg/mL in PBS, added to the previous solution). The reaction was carried out at 4 °C for another 24 h. The GAGs-coated surfaces were rinsed by copious amounts of PBS and Milli-Q water, dried with a stream of nitrogen, and then characterized by ζ-potential measurements (Figure S2, Supporting Information, Table 2) and X-ray photoelectron spectroscopy (XPS, Figure S3, Supporting Information, and Table 2) or used in the following experiments. All used solutions were filtered through a 0.2 μm filter in a laminar flow cabinet to avoid bacterial contaminations.

2.3. Microcontact Printing (μCP) of Proteins. We tested two proteins in this study: albumin (bovine serum albumin, BSA, pI = 4.7, Sigma-Aldrich) and fibronectin (human plasma fibronectin, FN, pI = 5.5−6, Gibco). μCP of BSA and FN was performed over substrates functionalized with ox-HA and ox-HEP as described below (Figure 2). Poly(dimethylsiloxane) (PDMS, Sylgard 184, Dow Corning, Scharlab) stamps were fabricated according to a procedure published elsewhere.[19] Briefly, silicon masters were microstructured by photolithography and dry etching processes (Figures 2A and S5, Supporting Information). A mixture of silicone elastomer/curing agent (10:1) was cast over silicon masters and placed at 60 °C overnight. After that, PDMS was carefully peeled off from the silicon master and cut into 1 cm^2 stamps. It must be noted that each stamp had three areas with size of 10 × 3.33 mm^2 that differ by the pattern period (Figure 2A, inset): each area had grooves with 5 μm depth and periods of 50, 100, or 200

DOI: 10.1021/acsami.5b02479
ACS Appl. Mater. Interfaces 2015, 7, 10034−10043

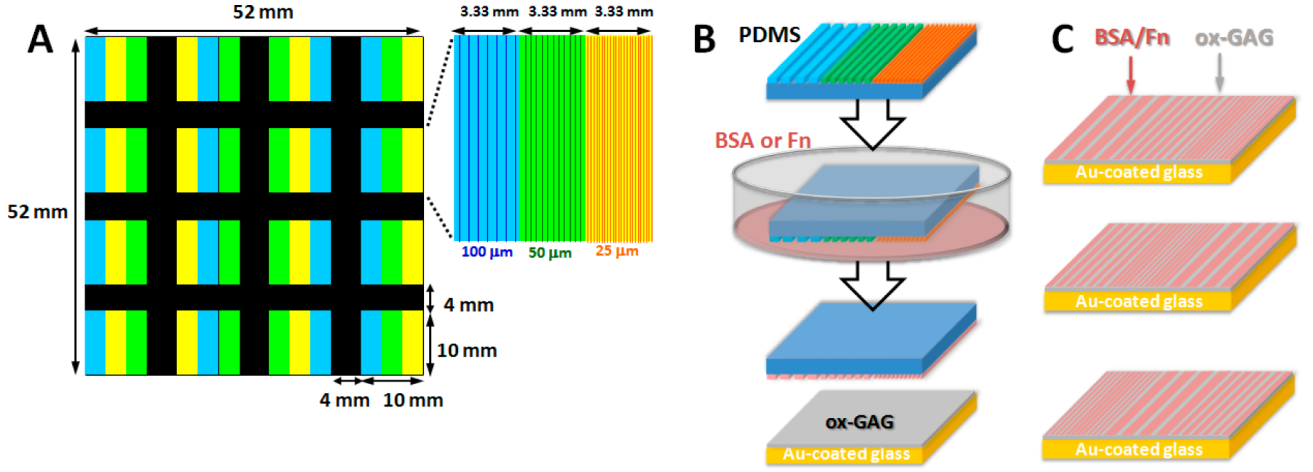

Figure 2. Schematic presentation of the used master (A), the obtained PDMS stamps and their use in μCP of proteins (BSA or FN) over ox-GAGs (B), and the generated patterns (C). The grooves with different widths are presented with different colors: 100 μm in blue, 50 μm in green, and 25 μm in orange.

μm, respectively. The positioning of these areas was different through the samples: our aim was to exclude artifacts in the cellular behavior caused by the seeding (there is a natural tendency to seed cells in the middle of the sample) but not as a result of the pattern size. The stamps were cleaned with 70% ethanol, sonicated for 5 min, and dried prior use.

Each PDMS stamp was incubated with 100 μL of sterile (filtered through a 0.2 um filter) BSA or FN (100 μg/mL) for 1 h. Afterward, the stamps were rinsed with water and dried under a N_2 flow.

The μCP was performed by placing the stamps over the substrates, applying a gentle pressure during 1 min, to get a conformal contact with the surfaces, and then carefully peeling them off (Figure 2B). Substrates were covered and stocked at 4 °C until cell seeding.

2.4. Isolation, Culture, and Characterization of Mesenchymal Stem Cells. We used mesenchymal stem cells from two sources: bone marrow and adipose tissue. While ASCs are the focus of this investigation, BMSCs were used as a control for comparison purposes since the stem cells from this source are the ones most studied.

Human bone marrow aspirates were obtained from healthy patients under the scope of a cooperation agreement with Hospital da Prelada (Porto, Portugal). BMSCs were separated on a Histopaque density gradient (1.077g/mL, Sigma-Aldrich) and washed with isotonic phosphate buffered saline solution (PBS, Sigma-Aldrich). BMSCs were expanded in α-modified Eagle's medium (α-MEM, Sigma-Aldrich) supplemented with 1% antibiotic/antimycotic (Gibco), 10% fetal bovine serum (FBS, Gibco), and 2 ng/mL bFGF. Cells from second to fourth passage were used in this study.

Human subcutaneous adipose tissue samples (age range of 20−36 years) were obtained from lipoaspiration procedures under the scope of a cooperation agreement with Hospital da Prelada (Porto, Portugal). The adipose tissue was washed with PBS containing 10% antibiotic/antimycotic and then digested with a 0.1% collagenase from *Clostridium histolyticum* (Sigma-Aldrich) solution in PBS for 45 min at 37 °C under gentle stirring. The digested tissue was gently pressed through a strainer and centrifuged at 1000*g* for 10 min. The cell pellet was resuspended and incubated in lysis buffer (155 mM NH_4Cl, 5.7 mM K_2HPO_4, 0.1 mM EDTA) 10 min before centrifugation at 800*g* for 10 min. Cells were expanded in α-modified Eagle's medium (Sigma-Aldrich) supplemented with 1% antibiotic/antimycotic (Gibco), 10% FBS (Gibco). Cells from third and fourth passage were used in this study. Both populations were characterized by flow cytometry prior to use (Figure S4, Supporting Information).

Micropatterned and control ox-GAGs coated surfaces (n = 3 for each condition) were seeded with MSCs at concentration of 3000 cells/cm^2 in serum free medium and incubated for 1, 7, and 24 h at 37 °C under a humidified atmosphere of 5% CO_2. The samples were washed twice with PBS, fixed in 10% neutral buffered formalin for 30 min at 4 °C, permeabilized with 0.2% Triton X-100 in PBS for 5 min, and blocked with 3% BSA in PBS for 30 min at room temperature. Phalloidin−TRITC conjugate was used (1:200 in PBS for 30 min, Sigma) to assess cytoskeleton organization. Nuclei were counterstained with 1 μg/mL 4,6-diamidina-2-phenylin (DAPI, Sigma) for 30 min. Primary antibody against vinculin (clone h-VIN1, 1:400 in 1% w/v BSA/PBS, Sigma), followed by rabbit antimouse Alexafluor-488 (1:500 in 1% w/v BSA/PBS, Invitrogen), was used to observe focal adhesion formation. Immunostaining was also employed to evaluate CD44 expression (HA receptor): the samples were incubated with a monoclonal CD44 antibody (8E2F3 clone, 1:500 in 1% w/v BSA/PBS, Acris) followed by rabbit antimouse Alexafluor-488 (1:500 in 1% w/v BSA/PBS, Invitrogen). Samples were washed with PBS, mounted with Vectashield (Vector) in glass slides, and observed under an Imager Z1 fluorescence microscope (Zeiss) and photographed using an Axio Cam MRm (Zeiss).

Morphology of the cultured cells was evaluated by scanning electron microscopy (SEM). The samples used for immunostaining were washed twice in PBS, dehydrated in a graded series of ethanol, dried using hexamethyldisilazane, and then examined at an accelerating voltage of 15 kV in a Leica Cambridge S-360 scanning electron microscope.

2.5. Morphometric Studies. The effect of the patterns on the cellular behavior (adhesion and morphology) was evaluated by observing changes in number of adherent cells per area and analyzing their shape. ImageJ software object tools were used to measure and compare the cell circularity. Postimage processing was applied to obtain a binary image where individual cells were identified. At least five circularity bins of 0.1 intervals were set up, and circularity values between 0 and 1 were placed in each bin (0 being a line and 1 being a circle). Cell orientation angle was analyzed using Orientation J plug-in. The morphometric analysis was performed using ImageJ 1.49e.

2.6. Statistical Analysis. All the quantitative results were obtained after analysis of at least three measurements per sample. Initially, a Shapiro−Wilk test was used to validate the normality of the data. Student's t tests for independent samples were performed to test differences among the samples. The results are presented as mean ± standard deviation (SD) if the data followed a normal distribution. Box plot presentation of the data is used when they did not follow a normal distribution. Kruskal−Wallis test followed by Mann−Whitney test was applied in this case in order to determine the statistical significance of the observed differences. Throughout the following discussion, the differences were considered significant if $p < 0.05$.

DOI: 10.1021/acsami.5b02479
ACS Appl. Mater. Interfaces 2015, 7, 10034−10043

3. RESULTS AND DISCUSSION

3.1. GAGs Functionalized Surfaces. The approaches used for immobilization of glycans on solid supports can be divided in two groups: (i) noncovalent deposition of high molecular weight polysaccharides on functionalized surfaces and (ii) methods based on covalent attachment of carbohydrates to the solid support. The main advantage of the strategies involving noncovalent immobilization is the possibility to use natural carbohydrates without any modification. The obtained surfaces are distinguished with an easy adjustment of the glycan binding sites because of the higher flexibility of the macromolecules on the supports. However, in our approach where a subsequent μCP is involved, the stability of the attached carbohydrate layer is the main concern, and thus, we have chosen the covalent immobilization. Among the different possibilities, the Schiff reaction is a convenient choice because it is straightforward, relatively fast, and cheap. Moreover, previous studies have demonstrated that this modification results in homogeneous distribution of GAG on amino-functionalized surfaces.[20] Generally, the approaches based on covalent immobilization require modification of both the used support and the carbohydrate to be attached.[21] The used carbohydrates therefore were oxidized to reactive aldehydes (Table 1, Figure S1, Supporting Information), and the supports were functionalized with the complementary amino-groups via self-assembled monolayers. The characterization of ox-GAGs by UV−vis showed approximately a 25% degree of oxidation for ox-HEP and a lower degree (~18%) for ox-HA (Table 1). This difference is in agreement with previous results, and it is explained with the less exposed/hindered by hydrogen bonds −OH groups of HA.[22] Functionalization of biopolymers often results in side hydrolysis; oxidation of GAGs with $NaIO_4$ causes cleavage of glycoside bonds, and a decrease of the M_w for both studied GAGs was observed (HA: from 1.3 MDa to 160 kDa; HEP: from 15 to 9 kDa).

Table 1. Characteristics of Oxidized Glycosaminoglycans

sample	Ds[a]	Do (%)[b]	CHO content ($\times 10^{-4}$ mol/g)[b]	M_w (kDa)[c]	M_n (kDa)[c]	PDI[c]
Ox-HA		17.5	9.0	160	100	1.5
Ox-HEP	1.3	25.5	14.5	9	6	1.5

[a]Degree of sulfation (Ds) was determined by elemental analysis. [b]Aldehyde content was determined using Schiff's reagent via UV−vis spectroscopy. The degree of oxidation (Do) was calculated from the experimental aldehyde content in relation to the molar amount of GAGs disaccharide repeating units. [c]Weight-average (M_w) and number-average (M_n) molecular weight of oxidized molecules was determined by flow field-flow fractionation (FFFF) with mobile phase 50 mM NaCl. Molecular weight distribution (polydispersity index: PDI) is based on the values calculated from FFFF detection.

In the next step, we generated GAG-functionalized surfaces via a Schiff base reaction between the obtained ox-GAGs and substrates uniformly coated with $-NH_2$ groups (Figure 1). The functionalization of the NH_2 surfaces with GAGs was confirmed by several surface characterization techniques (Table 2, Figures S2 and S3, Supporting Information).

The charge of the surfaces decreased after their modification with GAGs: both points of zero charge (POZ) and zeta potential at pH 7.4 were significantly lower, which corresponds to the negatively charged carboxylic and sulfate groups of HA and HEP (Figure S2, Supporting Information). Finally, a new signal at 165−169 eV appeared for oxidized sulfur in the XPS of the HEP-functionalized surface (Figure S3, Supporting Information) also confirming the success of the Schiff reaction.

Table 2. Characteristics of the GAG-Functionalized Surfaces[a]

	XPS							
sample	Au	C	O	N	S	SH/SO_3	ZP at pH 7.4	POZ
−NH2	38.1	45.6	8.8	6.3	1.2	1:0	−32.5	6.1
ox-HA	32.8	47.9	10.4	5.4	3.5	0.8:0.2	−60.7	4.0
ox-HEP	25.5	51.7	13.5	4.2	5.0	0.5:0.5	−78.4	3.8

[a]Used abbreviations: ZP, zeta potential; POZ, point of zero charge; ox-HA, oxidized hyaluronic acid; ox-HEP, oxidized heparin.

3.2. Cell Behavior on GAG-Functionalized Surfaces. The influence of HA on cellular response has been a subject of great interest in the last two decades.[23−25] It has been clearly demonstrated that the properties of HA, e.g., its molecular weight, influence significantly the behavior of cells in contact with this GAG:[26−29] generally, HA with high molecular weight is associated with low cell adhesion.[26,28,29] HEP also influences cell adhesion but the reported results are quite contradictory, suggesting that HEP bioactivity depends on the way of its incorporation.[30−36] We used bone marrow-mesenchymal stem cells (BMSCs) and adipose derived stem cells (ASCs) in contact with the GAG-functionalized surfaces and in the absence of any proteins to screen the effect of the immobilized GAGs on cell adhesion and morphology. Cells adhered to all studied surfaces after 1 h of culture regardless of the underlying GAG (ox-HA or ox-HEP). The surface chemistry did not influence the number of adherent cells, but cells from different sources behave otherwise: we observed significantly more adherent ASCs than BMSCs on all surfaces (Figure 3C). The morphology of BMSC and ASC was also different: ASCs were rounder than BMSCs, which formed long filopodia even at a very short culture time (Figure 3A,B 1 h). We applied cell morphometrics to quantify these observations. The results demonstrated that different surface chemistry influenced cells shape; however, significant changes were measured only for ASCs (Figure 3D). The immunostaining of the adherent ASCs and BMSCs revealed additional differences between these cells: formation of focal adhesions (FA) was observed for BMSCs only after 1 h of culture regardless of the used substrate (Figure 4A) while no FA were visible for ASCs at any of the studied culture times (Figure 4B). At longer culture times (7 and 24 h), the cells started to spread. The axial ratio and total spread area of MSCs were calculated using ImageJ 1.49e software. Although MSCs spreading area was similar on both surfaces (ox-HA and ox-HEP) after 24 h of culture (Figure 3E), on ox-HA surfaces, cells were significantly less stretched than on the corresponding ox-HEP surfaces (Figure 3F). The cytoskeleton organization was also influenced by the immobilized ox-GAG: ox-HEP induced formation of well pronounced actin fibers for the MSCs from both sources (Figure 4A, B). This difference can be explained by the ability of MSCs to secrete fibronectin,[37,38] which can further interact specifically with HEP (but not with HA). Indeed, previous studies have reported similar results: $-SO_3H$ groups induce distinct cytoskeleton organization in MSCs that may be related to the differentiation of those cells.[39−41]

DOI: 10.1021/acsami.5b02479
ACS Appl. Mater. Interfaces 2015, 7, 10034−10043

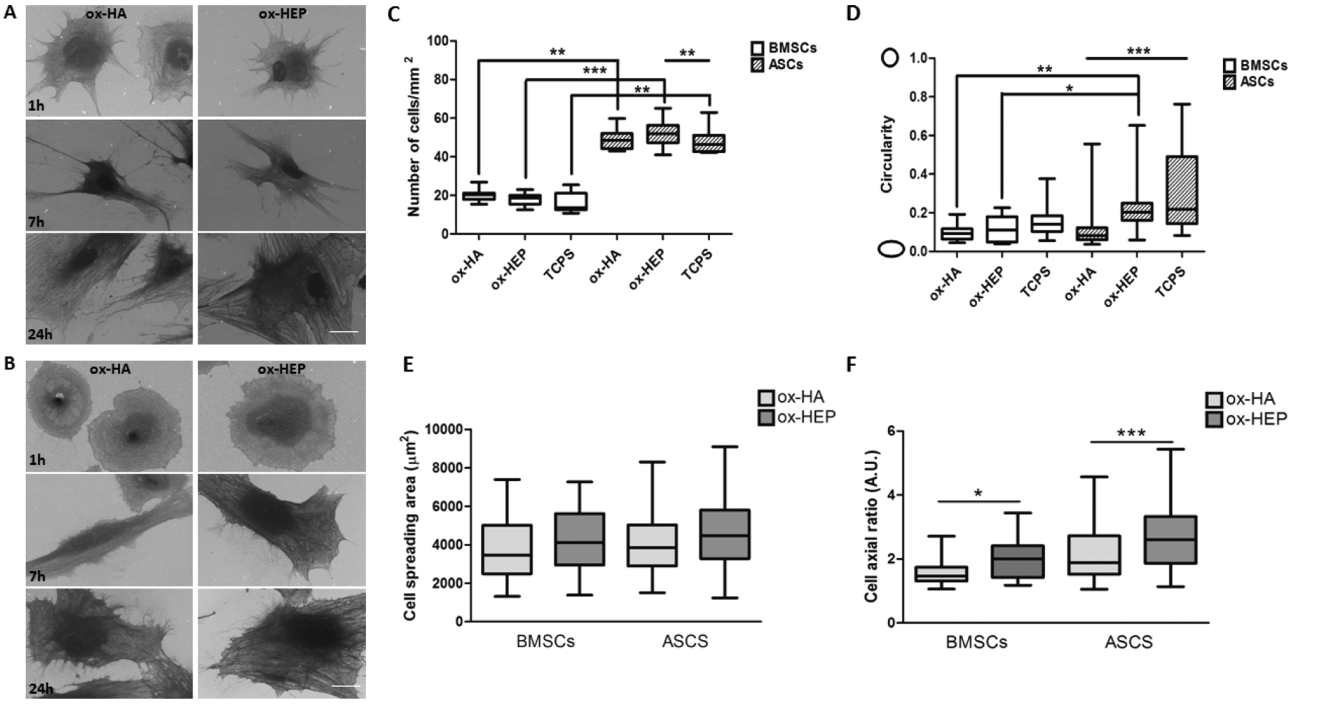

Figure 3. Analysis of adhesion and morphology of MSC cultured in contact with ox-GAGs functionalized surfaces: scanning electron micrographs (scale bars = 20 μm) showing the morphology of BMSCs (A) and ASCs (B) after different culture times. Analysis of cell adhesion after 1 h of culture showed significantly more adherent ASCs than BMSCs regardless of the used substrate (C). At this time point, the underlying ox-GAGs influenced significantly the morphology of ASCs but not that of BMSCs (D). Total cell surface area (E) and cell axial ratio (F) after 1 h of culture were quantified to evaluate cell spreading.The significant difference is marked with *** ($p \leq 0.001$), ** ($p \leq 0.01$), and * ($p \leq 0.05$).

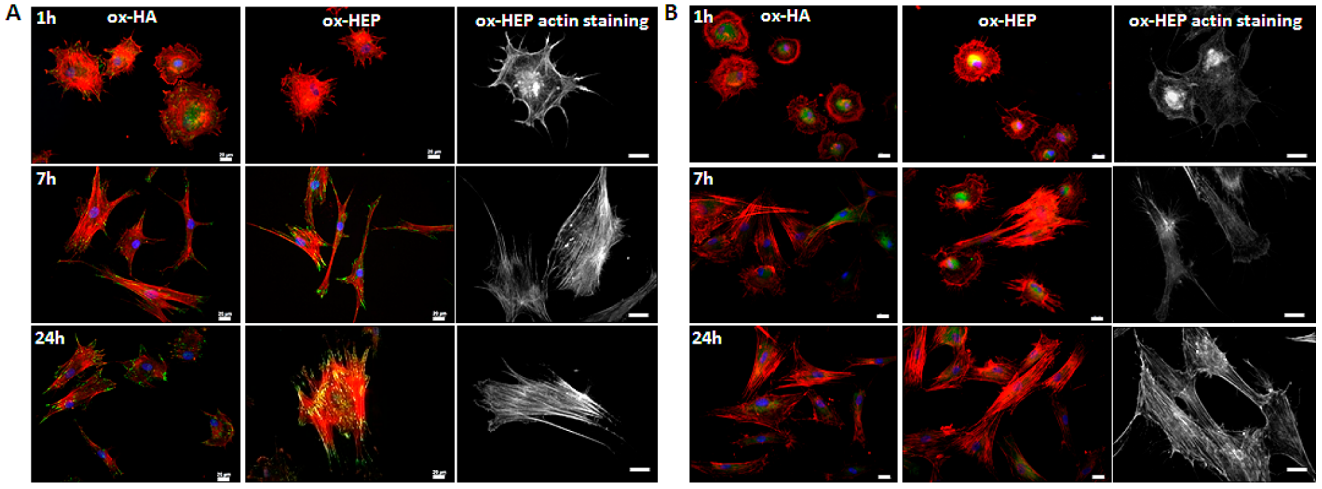

Figure 4. Fluorescence microscopy images showing cytoskeleton organization of BMSCs (A) and ASCs (B) after culture on ox-GAGs functionalized surfaces with different degrees of sulfation. Scale bars correspond to 20 μm. Immunostaining of vinculin (green), actin (red), and nuclei (blue).

3.3. Expression of CD44. CD44 comprises a single gene encoded family of glycoproteins with broad size heterogeneity (80−200 kDa) due to variable N- and O-linked glycosylation and to alternative splicing.[42] Different isoforms of CD44 have binding domains for GAGs (e.g HA, heparan sulfate) and other ECM components (e.g., collagen, laminin, and fibronectin).[42,43] CD44-mediated cell interaction with HA has been implicated in different physiological events including cell−cell and cell−substrate adhesion, migration, proliferation, and HA uptake and degradation. Several studies have reported that CD44 expression is one of the characteristics of *in vitro* culture of MSCs.[6,44] Indeed, a recent report suggests that primary MSCs and progenitor cells of bone marrow reside in the CD44-cell fraction that acquires CD44 expression after *in vitro* culture.[10,45] In fact, CD44−HA interactions have been implicated in MSCs adhesion and migration.[46,47] Both populations of MSCs used in this study were CD44+ (Figure S4, Supporting Information). We used immunocytochemistry to analyze the CD44 expression of BMSCs and ASCs cultured in contact with the ox-GAG-functionalized surfaces (Figure 5).

Shortly after seeding (1 h), CD44 levels for BMSCs were much higher than for ASCs regardless of the underlying surface (Figure 5A). Indeed, it has previously been shown that CD44 is expressed on BMSCs but not modulated by HA despite the higher content of this GAG in the ECM of the bone marrow stroma.[48] This data is in agreement with the results obtained by

DOI: 10.1021/acsami.5b02479
ACS Appl. Mater. Interfaces 2015, 7, 10034−10043

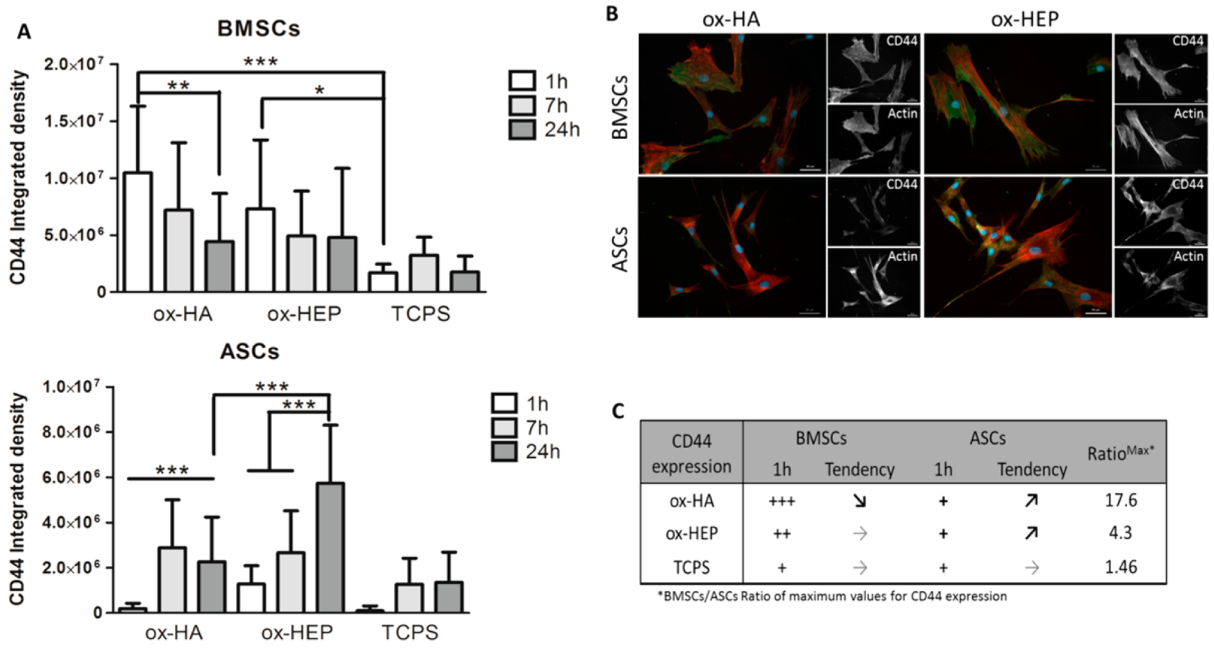

Figure 5. CD44 expression for BMSCs and ASCs cultured on GAG-functionalized surfaces. Integrated density values and significant differences are shown for all the time points (A). Fluorescence images (B) corresponding to the last time point (24 h) showing CD44 (green), cytoskeleton (red), and nuclei (blue). Single channel images are shown representing CD44 (green) and actin (red) staining. The ratio of BMSCs/ASCs maximum density values for CD44 after 1 h of culture is also presented (C). The significant difference is marked with *** ($p \leq 0.001$), ** ($p \leq 0.01$), and * ($p \leq 0.05$).

us and justified the high levels of CD44 detected for MSC from this source. The ECM of adipose tissue has a composition that is quite different from that of bone marrow stroma with HEP and chondroitin sulfate as the main GAG components.[49] This differential ECM composition most probably is reflected in the receptor expression by these cells.

Because CD44 is an HA receptor, we expected that CD44 expression will be modulated in MSCs cultured on ox-HA functionalized surfaces. Indeed, we observed a change in the CD44 expression for both ASCs and BMSCs with prolongation of the culture time, however, in opposite directions (Figure 5). In the case of BMSCs cultures, the initial CD44 levels remained stable throughout the whole experiment for ox-HEP-functionalized surfaces, as for the controls (TCPS). BMSCs cultured on surfaces functionalized with ox-HA expressed less CD44 with prolongation of the culture time although the obtained values were still higher than the maximum values detected for ASCs (Figure 5A,B). Opposite behavior was observed for ASCs cultures. In the beginning, CD44 levels were similar for all tested surfaces and they increased for longer culture times (7 and 24 h, Figure 5C). We, therefore, hypothesize that the mechanism for CD44 signal transduction is different in ASCs and BMSCs and is related to the different ECM composition of these cells already discussed above.

It must be noted that CD44 expression increased for ASCs cultured on ox-HA but also on ox-HEP functionalized surfaces. It is known that low molecular weight HEP (as the one used by us) can induce an increase in CD44 expression in mice.[50] Moreover, HEP-responsive CD44 isoforms are described for trophoblast and cancer cells[43,51] and such isoforms may also be expressed by ASCs.

3.4. Protein-GAGs Patterned Surfaces. The possibility to control cell adhesion, differentiation, and assembly on 2D culture substrates via different micro- and nanoscale patterns has been the subject of intensive research in the last decades.[52] Several soft lithography techniques have been developed to create such functional patterns. Among different possibilities, we have chosen the simplest and cost-effective μCP (Figure 2B) to generate patterns on the ox-GAG functionalized surfaces applying a procedure previously described by us.[19] μCP techniques are powerful tools to print molecules on reactive surfaces in a covalent or noncovalent manner to produce well-defined (both shape and spot morphology) patterns of bioactive molecules.[14] The functionality of the patterns can be tuned by adjusting several parameters such as patterned molecules and the period and the depth of the pattern as well as its shape. As patterned molecules, we used two proteins: albumin is an abundant, relatively small, and globular protein, preventing cell attachment, while fibronectin is a cell-adhesive protein that binds to one of the used GAG in this study, HEP, via its specific heparin-binding domains.[53] Different periods of the pattern were also tested (Figures S5 and S6, Supporting Information). Previous studies have demonstrated that cells may switch between growth, apoptosis, and differentiation as a function of the pattern width:[54,55] small pattern widths (<10 μm) can prevent cell attachment, while very wide patterns (>200 μm) may act as a nonpatterned surface, i.e., cells do not recognize the pattern and do not align.[54]

The stability of the patterns generated by us was confirmed using labeled proteins (BSA and FN): all patterns were stable after washing the samples several times with phosphate buffer saline (PBS, Figure S6, Supporting Information). The effect of the patterning over MSCs behavior was evaluated using only ASCs, on the basis of our results with nonpatterned surfaces (more attached cells and a significantly different response of those cells to underlying ox-GAGs). The cells rapidly adhered to all studied surfaces (1 h) and began to align on the substrates (7 h) regardless of the used ox-GAG and protein (Figures S7, Supporting Information, 6, and 7B).

DOI: 10.1021/acsami.5b02479
ACS Appl. Mater. Interfaces 2015, 7, 10034−10043

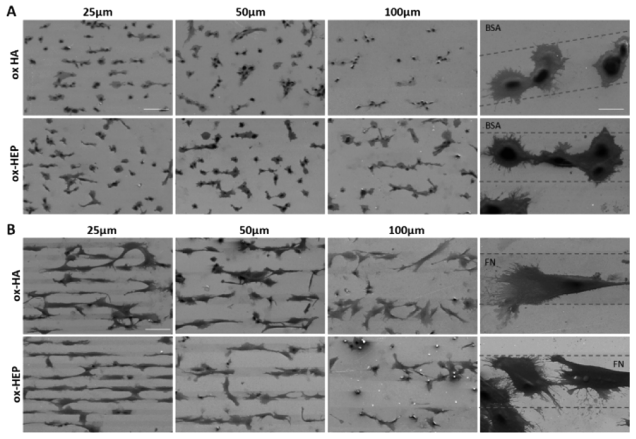

Figure 6. Attachment of ASCs on ox-GAG surfaces patterned with BSA (A) and FN (B), after 7 h of culture. Darker regions in the SEM images correspond to the protein pattern. Bars correspond to 100 μm (low magnification images) and 20 μm (high magnification images).

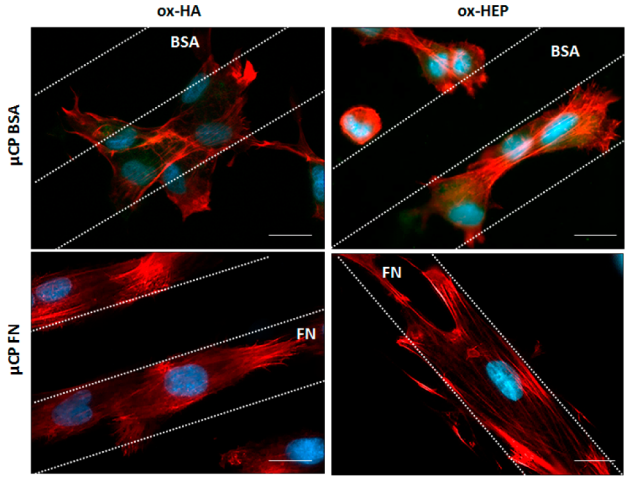

Figure 8. CD44 expression for ASCs cultured on ox-GAG surfaces patterned with BSA and FN after 7 h of culture. Fluorescence images showing CD44 (green), cytoskeleton (red), and nuclei (blue). Bars correspond to 20 μm.

More attached cells and the best alignment were observed for the smallest pattern (25 μm) and smears with an increase in the pattern size. Cell bridging is also evident for the smallest pattern (25 μm), and it decreased with an increase in the pattern size (Figure 6). The morphometric analysis confirmed these observations (Figure 7A). When FN was patterned, cells adhered to the protein functionalized areas (darker on the SEM micrographs) and developed a cytoskeleton with well-structured actin fibers and extended lamellipodia which were mostly restricted to the protein patterned area (Figures 6B and 8).

We did not observe any significant effect of the pattern size over cell circularity for these patterns (Figure 7A). Several studies demonstrated enhanced cell attachment and spreading on homogeneously FN-coated surfaces compared to identical materials in the absence of FN.[56−61] We however did not observe such spreading effect for FN patterned surfaces: cell shape of ASCs cultured on nonpatterned (ox-GAG) surfaces was similar to the cultures in contact with FN patterns (Figure 7A). A possible reason for this result is the size of the ASCs: they are relatively big cells as their size is comparable with the size of the patterns. As a result, the cytoskeleton of a single cell is enough to cover all the width of the FN-coated area, i.e., the spreading of a single cell is limited by the width of the pattern. Protein patterning affected the alignment of cells on all surfaces (Figure 7B).

Cell orientation depended on both pattern width and patterned protein: the best alignment (lower orientation angles) was observed for the samples with the smallest FN pattern width (25, 50 μm) (Figure 7B). The underlying GAG is also important: ASCs cultured in contact with FN patterns on ox-HEP had better orientation than those cultured on FN patterned ox-HA ($p \leq 0.001$) (Figure 7). None of these effects were observed for the BSA patterned surfaces. A closer look at the SEM pictures revealed that, when the BSA was patterned, cells adhered to the GAG exposed areas (Figure 6A) and had morphology that is quite different from the one observed for ASCs adherent on ox-GAG surfaces without pattern; i.e., although the cells do not interact directly with the patterned protein, its presence affects ASCs morphology. Different morphology and cytoskeletal organization often can lead to a differentiation process or can be an indicator for the occurrence of such process. ASCs seeded on BSA patterned surfaces had significantly rounder shape (Figure 7A). Besides different morphology, ASCs adherent to the ox-GAG areas were positive for CD44 while ASCs adherent on FN patterns did not express CD44 (Figure 8). The different morphology together with

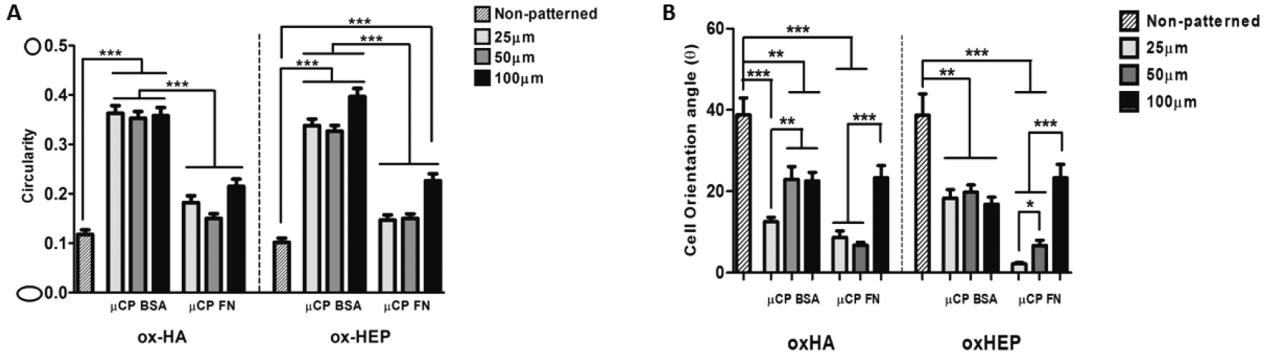

Figure 7. Morphometric analysis of ASCs after 7 h in culture. Analysis of ASCs at the cellular level shows significant differences in circularity between nonpatterned and patterned surfaces (A). Significant differences were detected for the two protein patterns (BSA and FN) and for the different pattern widths (25, 50, and 100 μm). ASCs cultured on surfaces containing FN and ox-HEP show different cell orientation angles depending on the pattern widths (B). The significant difference ($p \leq 0.001$, $p \leq 0.01$, and $p \leq 0.05$) is marked with ***, **, and *, respectively.

DOI: 10.1021/acsami.5b02479
ACS Appl. Mater. Interfaces 2015, 7, 10034−10043

expression of different surfaces markers and the well documented ability of ASCs to differentiate into different lineages suggested that these surfaces can lead to differentiation of ASCs.

4. CONCLUSIONS

Advances in nano- and microscale technologies made available different strategies to engineer cell alignment including mechanical loadings, topographical patterning, surface chemical treatment, or a combination of these approaches. As a result of these strategies, cell alignment can be promoted through either mechanical modulation of the cytoskeleton or directive physical and/or chemical gradients within local ECMs. Indeed, we demonstrated that cells were able to respond to the external stimuli and underwent an adaptive process dependent on cell signaling and communication, during which cytoskeleton reorganization and directional cell spreading occurred. Furthermore, the results obtained with our platforms showed that on smaller pattern widths cell bridging occurred more frequently, which could be useful for applications that require cell−cell interactions between patterns or formation of cell sheets, without disturbing cell alignment.[62] The combination of ox-GAGs and μCP could also be used for MSCs differentiation into different lineages, given the importance of the ECM environment for the regulation of differentiation and development.[63,64]

Our data demonstrated a double role of the developed surfaces in the control of cell morphology and expression of different markers: cell−surface interactions were substantially affected not only by the surface topography but also by the pattern chemical composition. Further studies that include patterning of different matrix proteins (e.g., collagen, laminin) and growth factors or more than one protein will be of high relevance for elucidating the complex communication between cells and their closest environment.

■ ASSOCIATED CONTENT

Supporting Information

Experimental details and characterization data. The Supporting Information is available free of charge on the ACS Publications website at DOI: 10.1021/acsami.5b02479.

■ AUTHOR INFORMATION

Corresponding Authors

*E-mail: diana.costa@dep.uminho.pt. Tel: +351 253 510907.
*E-mail: pashkuleva@dep.uminho.pt. Tel.: +351 253 510907.

Notes

The authors declare no competing financial interest.

■ ACKNOWLEDGMENTS

This work was carried out under the scope of the EU seventh Framework Programme (FP7/2007-2013) under grant agreement no. NMP4-SL-2009-229292 (Find&Bind). D.S.C. and I.P. acknowledge the Portuguese Foundation for Science and Technology (FCT) for their grants (BPD/85790/2012 and IF/00032/2013).

■ REFERENCES

(1) Petrakova, K. V.; Tolmacheva, A. A.; Friedenstein, A. J. Bone Formation Occurring in Bone Marrow Transplantation in Diffusion Chambers. *Bull. Exp. Biol. Med.* **1963**, *56*, 87−91.

(2) Bianco, P.; Cao, X.; Frenette, P. S.; Mao, J. J.; Robey, P. G.; Simmons, P. J.; Wang, C. Y. The Meaning, the Sense and the Significance: Translating the Science of Mesenchymal Stem Cells into Medicine. *Nat. Med.* **2013**, *19*, 35−42.

(3) Kfoury, Y.; Scadden, D. T. Mesenchymal Cell Contributions to the Stem Cell Niche. *Cell Stem Cell* **2015**, *16*, 239−253.

(4) Baer, P. C.; Geiger, H. Adipose-Derived Mesenchymal Stromal/Stem Cells: Tissue Localization, Characterization, and Heterogeneity. *Stem Cells Int.* **2012**, 11.

(5) Strem, B. M.; Hicok, K. C.; Zhu, M.; Wulur, I.; Alfonso, Z.; Schreiber, R. E.; Fraser, J. K.; Hedrick, M. H. Multipotential Differentiation of Adipose Tissue-Derived Stem Cells. *Keio J. Med.* **2005**, *54*, 132−141.

(6) Zuk, P. A.; Zhu, M.; Ashjian, P.; De Ugarte, D. A.; Huang, J. I.; Mizuno, H.; Alfonso, Z. C.; Fraser, J. K.; Benhaim, P.; Hedrick, M. H. Human Adipose Tissue Is a Source of Multipotent Stem Cells. *Mol. Biol. Cell* **2002**, *13*, 4279−4295.

(7) Strioga, M.; Viswanathan, S.; Darinskas, A.; Slaby, O.; Michalek, J. Same or not the Same? Comparison of Adipose Tissue-Derived versus Bone Marrow-Derived Mesenchymal Stem and Stromal Cells. *Stem Cells Dev.* **2012**, *21*, 2724−2752.

(8) Docheva, D.; Haasters, F.; Schieker, M. Mesenchymal Stem Cells and Their Cell Surface Receptors. *Curr. Rheumatol. Rev.* **2008**, *4*, 155−160.

(9) Gimble, J.; Guilak, F. Adipose-Derived Adult Stem Cells: Isolation, Characterization, and Differentiation Potential. *Cytotherapy* **2003**, *5*, 362−369.

(10) Mitchell, J. B.; McIntosh, K.; Zvonic, S.; Garrett, S.; Floyd, Z. E.; Kloster, A.; Di Halvorsen, Y.; Storms, R. W.; Goh, B.; Kilroy, G.; Wu, X.; Gimble, J. M. Immunophenotype of Human Adipose-Derived Cells: Temporal Changes in Stromal-Associated and Stem Cell-Associated Markers. *Stem Cells* **2006**, *24*, 376−385.

(11) Guilak, F.; Cohen, D. M.; Estes, B. T.; Gimble, J. M.; Liedtke, W.; Chen, C. S. Control of Stem Cell Fate by Physical Interactions with the Extracellular Matrix. *Cell Stem Cell* **2009**, *5*, 17−26.

(12) Daley, W. P.; Peters, S. B.; Larsen, M. Extracellular Matrix Dynamics in Development and Regenerative Medicine. *J. Cell Sci.* **2008**, *121*, 255−264.

(13) von der Mark, K.; Park, J. Engineering Biocompatible Implant Surfaces Part II: Cellular Recognition of Biomaterial Surfaces: Lessons from Cell-Matrix Interactions. *Prog. Mater. Sci.* **2013**, *58*, 327−381.

(14) Voskuhl, J.; Brinkmann, J.; Jonkheijm, P. Advances in Contact Printing Technologies of Carbohydrate, Peptide and Protein Arrays. *Curr. Opin. Chem. Biol.* **2014**, *18*, 1−7.

(15) Hsiao, T. W.; Swarup, V. P.; Eichinger, C. D.; Hlady, V. Cell Substrate Patterning with Glycosaminoglycans to Study Their Biological Roles in the Central Nervous System. *Methods Mol. Biol. (Clifton, NJ)* **2015**, *1229*, 457−467.

(16) Castano, A. G.; Hortiguela, V.; Lagunas, A.; Cortina, C.; Montserrat, N.; Samitier, J.; Martinez, E. Protein Patterning on Hydrogels by Direct Microcontact Printing: Application to Cardiac Differentiation. *RSC Adv.* **2014**, *4*, 29120−29123.

(17) Pankov, R.; Yamada, K. M. Fibronectin at a Glance. *J. Cell Sci.* **2002**, *115*, 3861−3863.

(18) Wang, D. A.; Varghese, S.; Sharma, B.; Strehin, I.; Fermanian, S.; Gorham, J.; Fairbrother, D. H.; Cascio, B.; Elisseeff, J. H. Multifunctional Chondroitin Sulphate for Cartilage Tissue-Biomaterial Integration. *Nat. Mater.* **2007**, *6*, 385−392.

(19) Marquez-Posadas, M. C.; Ramiro, J.; Becher, J.; Yang, Y.; Kowitsch, A.; Pashkuleva, I.; Diez-Ahedo, R.; Schnabelrauch, M.; Reis, R. L.; Groth, T.; Merino, S. Surface Microstructuring and Protein Patterning Using Hyaluronan Derivatives. *Microelectron. Eng.* **2013**, *106*, 21−26.

(20) Kowitsch, A.; Yang, Y.; Ma, N.; Kuntsche, J.; Mader, K.; Groth, T. Bioactivity of Immobilized Hyaluronic Acid Derivatives Regarding Protein Adsorption and Cell Adhesion. *Biotechnol. Appl. Biochem.* **2011**, *58*, 376−389.

(21) Pashkuleva, I.; Reis, R. L. Sugars: Burden or Biomaterials of the Future? *J. Mater. Chem.* **2010**, *20*, 8803−8818.

DOI: 10.1021/acsami.5b02479
ACS Appl. Mater. Interfaces 2015, 7, 10034−10043

(22) Morra, M. Engineering of Biomaterials Surfaces by Hyaluronan. *Biomacromolecules* **2005**, *6*, 1205−1223.
(23) Barbucci, R.; Magnani, A.; Lamponi, S.; Pasqui, D.; Bryan, S. The Use of Hyaluronan and Its Sulphated Derivative Patterned with Micrometric Scale on Glass Substrate in Melanocyte Cell Behaviour. *Biomaterials* **2003**, *24*, 915−926.
(24) Barbucci, R.; Torricelli, P.; Fini, M.; Pasqui, D.; Favia, P.; Sardella, E.; d'Agostino, R.; Giardino, R. Proliferative and Re-Defferentiative Effects of Photo-Immobilized Micro-Patterned Hyaluronan Surfaces on Chondrocyte Cells. *Biomaterials* **2005**, *26*, 7596−7605.
(25) Khademhosseini, A.; Suh, K. Y.; Yang, J. M.; Eng, G.; Yeh, J.; Levenberg, S.; Langer, R. Layer-by-Layer Deposition of Hyaluronic Acid and Poly-L-Lysine for Patterned Cell Co-Cultures. *Biomaterials* **2004**, *25*, 3583−3592.
(26) Kouvidi, K.; Berdiaki, A.; Nikitovic, D.; Katonis, P.; Afratis, N.; Hascall, V. C.; Karamanos, N. K.; Tzanakakis, G. N. Role of Receptor for Hyaluronic Acid-Mediated Motility (RHAMM) in Low Molecular Weight Hyaluronan (LMWHA)-Mediated Fibrosarcoma Cell Adhesion. *J. Biol. Chem.* **2011**, *286*, 38509−38520.
(27) Yang, C.; Cao, M.; Liu, H.; He, Y.; Xu, J.; Du, Y.; Liu, Y.; Wang, W.; Cui, L.; Hu, J.; Gao, F. The High and Low Molecular Weight Forms of Hyaluronan Have Distinct Effects on CD44 Clustering. *J. Biol. Chem.* **2012**, *287*, 43094−43107.
(28) Morra, M.; Cassinelli, C.; Carpi, A.; Giardino, R.; Fini, M. Effects of Molecular Weight and Surface Functionalization on Surface Composition and Cell Adhesion to Hyaluronan Coated Titanium. *Biomed. Pharmacother.* **2006**, *60*, 365−369.
(29) Liu, C. M.; Yu, C. H.; Chang, C. H.; Hsu, C. C.; Huang, L. L. Hyaluronan Substratum Holds Mesenchymal Stem Cells in Slow-Cycling Mode by Prolonging G1 Phase. *Cell Tissue Res.* **2008**, *334*, 435−443.
(30) Kim, M.; Kim, Y.-J.; Gwon, K.; Tae, G. Modulation of Cell Adhesion of Heparin-Based Hydrogel by Efficient Physisorption of Adhesive Proteins. *Macromol. Res.* **2012**, *20*, 271−276.
(31) Kreke, M. R.; Badami, A. S.; Brady, J. B.; Akers, R. M.; Goldstein, A. S. Modulation of Protein Adsorption and Cell Adhesion by Poly(allylamine hydrochloride) Heparin Films. *Biomaterials* **2005**, *26*, 2975−2981.
(32) Aggarwal, N.; Altgarde, N.; Svedhem, S.; Michanetzis, G.; Missirlis, Y.; Groth, T. Tuning Cell Adhesion and Growth on Biomimetic Polyelectrolyte Multilayers by Variation of pH During Layer-by-Layer Assembly. *Macromol. Biosci.* **2013**, *13*, 1327−1338.
(33) Kirchhof, K.; Andar, A.; Yin, H. B.; Gadegaard, N.; Riehle, M. O.; Groth, T. Polyelectrolyte Multilayers Generated in a Microfluidic Device with pH Gradients Direct Adhesion and Movement of Cells. *Lab Chip* **2011**, *11*, 3326−3335.
(34) Kirchhof, K.; Hristova, K.; Krasteva, N.; Altankov, G.; Groth, T. Multilayer Coatings on Biomaterials for Control of MG-63 Osteoblast Adhesion and Growth. *J. Mater. Sci.: Mater. Med.* **2009**, *20*, 897−907.
(35) Benoit, D. S.; Durney, A. R.; Anseth, K. S. The Effect of Heparin-Functionalized PEG Hydrogels on Three-Dimensional Human Mesenchymal Stem Cell Osteogenic Differentiation. *Biomaterials* **2007**, *28*, 66−77.
(36) Park, I.-S.; Han, M.; Rhie, J.-W.; Kim, S. H.; Jung, Y.; Kim, I. H.; Kim, S.-H. The Correlation Between Human Adipose-Derived Stem Cells Differentiation and Cell Adhesion Mechanism. *Biomaterials* **2009**, *30*, 6835−6843.
(37) Walter, M. N. M.; Wright, K. T.; Fuller, H. R.; MacNeil, S.; Johnson, W. E. B. Mesenchymal Stem Cell-Conditioned Medium Accelerates Skin Wound Healing: An in Vitro Study of Fibroblast and Keratinocyte Scratch Assays. *Exp. Cell Res.* **2010**, *316*, 1271−1281.
(38) Alexeev, V.; Arita, M.; Donahue, A.; Bonaldo, P.; Chu, M.-L.; Igoucheva, O. Human Adipose-Derived Stem Cell Transplantation as a Potential Therapy for Collagen VI-Related Congenital Muscular Dystrophy. *Stem Cell Res. Ther.* **2014**, *5*, 21.
(39) Soares da Costa, D.; Pires, R. A.; Frias, A. M.; Reis, R. L.; Pashkuleva, I. Sulfonic Groups Induce Formation of Filopodia in Mesenchymal Stem Cells. *J. Mater. Chem.* **2012**, *22*, 7172−7178.
(40) Büttner, M.; Möller, S.; Keller, M.; Huster, D.; Schiller, J.; Schnabelrauch, M.; Dieter, P.; Hempel, U. Over-Sulfated Chondroitin Sulfate Derivatives Induce Osteogenic Differentiation of hMSC Independent of BMP-2 and TGF-β1 Signalling. *J. Cell. Physiol.* **2013**, *228*, 330−340.
(41) Kliemt, S.; Lange, C.; Otto, W.; Hintze, V.; Möller, S.; von Bergen, M.; Hempel, U.; Kalkhof, S. Sulfated Hyaluronan Containing Collagen Matrices Enhance Cell-Matrix-Interaction, Endocytosis, and Osteogenic Differentiation of Human Mesenchymal Stromal Cells. *J. Proteome Res.* **2012**, *12*, 378−389.
(42) Marhaba, R.; Zöller, M. CD44 in Cancer Progression: Adhesion, Migration and Growth Regulation. *J. Mol. Histol.* **2004**, *35*, 211−231.
(43) Suga, N.; Sugimura, M.; Koshiishi, T.; Yorifuji, T.; Makino, S.; Takeda, S. Heparin/Heparan Sulfate/CD44-v3 Enhances Cell Migration in Term Placenta-Derived Immortalized Human Trophoblast Cells. *Biol. Reprod.* **2012**, *86* (134), 1−8.
(44) Hass, R.; Kasper, C.; Bohm, S.; Jacobs, R. Different Populations and Sources of Human Mesenchymal Stem Cells (MSC): A Comparison of Adult and Neonatal Tissue-Derived MSC. *Cell Commun. Signaling* **2011**, *9*, 12.
(45) Qian, H.; Le Blanc, K.; Sigvardsson, M. Primary Mesenchymal Stem and Progenitor Cells from Bone Marrow Lack Expression of CD44 Protein. *J. Biol. Chem.* **2012**, *287*, 25795−25807.
(46) Zhu, H.; Mitsuhashi, N.; Klein, A.; Barsky, L. W.; Weinberg, K.; Barr, M. L.; Demetriou, A.; Wu, G. D. The Role of the Hyaluronan Receptor CD44 in Mesenchymal Stem Cell Migration in the Extracellular Matrix. *Stem Cells* **2006**, *24*, 928−935.
(47) Solis, M. A.; Chen, Y.-H.; Wong, T. Y.; Bittencourt, V. Z.; Lin, Y.-C.; Huang, L. L. H. Hyaluronan Regulates Cell Behavior: A Potential Niche Matrix for Stem Cells. *Biochem. Res. Int.* **2012**, *2012*, 11.
(48) Lisignoli, G.; Cristino, S.; Piacentini, A.; Cavallo, C.; Caplan, A. I.; Facchini, A. Hyaluronan-Based Polymer Scaffold Modulates the Expression of Inflammatory and Degradative Factors in Mesenchymal Stem Cells: Involvement of CD44 and CD54. *J. Cell Physiol.* **2006**, *207*, 364−373.
(49) Mariman, E. M.; Wang, P. Adipocyte Extracellular Matrix Composition, Dynamics and Role in Obesity. *Cell. Mol. Life Sci.* **2010**, *67*, 1277−1292.
(50) Zhao, G.; Shaik, R. S.; Zhao, H.; Beagle, J.; Kuo, S.; Hales, C. A. Low Molecular Weight (LMW) Heparin Inhibits Injury-Induced Femoral Artery Remodeling in Mouse via Upregulating CD44 Expression. *J. Vasc. Surg.* **2011**, *53*, 1359−1367.e3.
(51) Jackson, D. G.; Bell, J. I.; Dickinson, R.; Timans, J.; Shields, J.; Whittle, N. Proteoglycan Forms of the Lymphocyte Homing Receptor CD44 Are Alternatively Spliced Variants Containing the v3 Exon. *J. Cell Biol.* **1995**, *128*, 673−685.
(52) Nikkhah, M.; Edalat, F.; Manoucheri, S.; Khademhosseini, A. Engineering Microscale Topographies to Control the Cell-Substrate Interface. *Biomaterials* **2012**, *33*, 5230−5246.
(53) Ruoslahti, E.; Hayman, E. G.; Engvall, E.; Cothran, W. C.; Butler, W. T. Alignment of Biologically Active Domains in the Fibronectin Molecule. *J. Biol. Chem.* **1981**, *256*, 7277−7281.
(54) Dike, L. E.; Chen, C. S.; Mrksich, M.; Tien, J.; Whitesides, G. M.; Ingber, D. E. Geometric Control of Switching Between Growth, Apoptosis, and Differentiation During Angiogenesis Using Micropatterned Substrates. *In Vitro Cell. Dev. Biol.: Anim.* **1999**, *35*, 441−448.
(55) Wan, L. Q.; Kang, S. M.; Eng, G.; Grayson, W. L.; Lu, X. L.; Huo, B.; Gimble, J.; Guo, X. E.; Mow, V. C.; Vunjak-Novakovic, G. Geometric Control of Human Stem Cell Morphology and Differentiation. *Integr. Biol.* **2010**, *2*, 346−353.
(56) Barbucci, R.; Magnani, A.; Chiumiento, A.; Pasqui, D.; Cangioli, I.; Lamponi, S. Fibroblast Cell Behavior on Bound and Adsorbed Fibronectin onto Hyaluronan and Sulfated Hyaluronan Substrates. *Biomacromolecules* **2005**, *6*, 638−645.
(57) Garcia, A. J.; Ducheyne, P.; Boettiger, D. Cell Adhesion Strength Increases Linearly with Adsorbed Fibronectin Surface Density. *Tissue Eng.* **1997**, *3*, 197−206.

DOI: 10.1021/acsami.5b02479
ACS Appl. Mater. Interfaces 2015, 7, 10034−10043

(58) Keselowsky, B. G.; Collard, D. M.; Garcia, A. J. Integrin Binding Specificity Regulates Biomaterial Surface Chemistry Effects on Cell Differentiation. *Proc. Natl. Acad. Sci. U.S.A.* **2005**, *102*, 5953−5957.
(59) Lee, M. H.; Ducheyne, P.; Lynch, L.; Boettiger, D.; Composto, R. J. Effect of Biomaterial Surface Properties on Fibronectin−$\alpha 5\beta 1$ Integrin Interaction and Cellular Attachment. *Biomaterials* **2006**, *27*, 1907−1916.
(60) Miller, T.; Boettiger, D. Control of Intracellular Signaling by Modulation of Fibronectin Conformation at the Cell-Materials Interface. *Langmuir* **2003**, *19*, 1723−1729.
(61) Wang, R.; Clark, R. A. F.; Mosher, D. F.; Ren, X. D. Fibronectin's Central Cell-Binding Domain Supports Focal Adhesion Formation and Rho Signal Transduction. *J. Biol. Chem.* **2005**, *280*, 28803−28810.
(62) Kaji, H.; Takoh, K.; Nishizawa, M.; Matsue, T. Intracellular Ca2+ Imaging for Micropatterned Cardiac Myocytes. *Biotechnol. Bioeng.* **2003**, *81*, 748−751.
(63) Mathews, S.; Mathew, S. A.; Gupta, P. K.; Bhonde, R.; Totey, S. Glycosaminoglycans Enhance Osteoblast Differentiation of Bone Marrow Derived Human Mesenchymal Stem Cells. *J. Tissue Eng. Regener. Med.* **2014**, *8*, 143−152.
(64) Reilly, G. C.; Engler, A. J. Intrinsic Extracellular Matrix Properties Regulate Stem Cell Differentiation. *J. Biomech.* **2010**, *43*, 55−62.

DOI: 10.1021/acsami.5b02479
ACS Appl. Mater. Interfaces 2015, 7, 10034−10043